HHS Public Access

Author manuscript

J Magn Reson Imaging. Author manuscript; available in PMC 2023 September 11.

Published in final edited form as:

J Magn Reson Imaging. 2022 April ; 55(4): 1026–1042. doi:10.1002/jmri.27865.

Recent Advances in Radio-Frequency Coil Technologies: Flexible, Wireless, and Integrated Coil Arrays

Dean Darnell, PhD,

Trong-Kha Truong, PhD,

Allen W. Song, PhD*

Brain Imaging and Analysis Center, Duke University, Durham, North Carolina, USA

Abstract

Radio-frequency (RF) coils are to magnetic resonance imaging (MRI) scanners what eyes are to the human body. Because of their critical importance, there have been constant innovations driving the rapid development of RF coil technologies. Over the past four decades, the breadth and depth of the RF coil technology evolution have far exceeded the space allowed for this review article. However, these past developments have laid the very foundation on which some of the recent technical breakthroughs are built upon. Here, we narrow our focus on some of the most recent RF coil advances, specifically, on flexible, wireless, and integrated coil arrays. To provide a detailed review, we discuss the theoretical underpinnings, experimental implementations, promising results, as well as future outlooks covering these exciting topics. These recent innovations have greatly improved patient comfort and ease of scan, while also increasing the signal-to-noise ratio, image resolution, temporal throughput, and diagnostic and treatment accuracy. Together with advances in other MRI subfields, they will undoubtedly continue to drive the field forward and lead us to an ever more exciting future.

Level of Evidence: 5

Technical Efficacy: Stage 1

The field of magnetic resonance imaging (MRI) has, since its inception, been constantly driven by technological advances: the emergence of high-field scanners (3T and above) has greatly increased the sensitivity and spatial resolution for clinical diagnosis and contributed to the explosive growth of MRI over the past two decades; the discovery and rapid expansion of functional MRI (fMRI) research was made possible by strong gradient coils that enabled single-shot fast imaging; the recent advances in artificial intelligence (AI) have led to further improved imaging contrast and disease specificity. Central to these clinical and research advances is the radio-frequency (RF) coil technology, in particular the permeation of phased array RF coils. These array coils increase the imaging sensitivity, spatial resolution, and scan efficiency (via parallel imaging techniques such as SENSE, GRAPPA, etc.), and also provide the much needed rich spatial and phase information for AI algorithms to further improve image contrast and sharpness.

*Address reprint requests to: A.W.S., 40 Duke Medicine Circle, Room 414, Durham, NC 27710, USA. allen.song@duke.edu.

Indeed, RF coils to MRI scanners are like eyes to the human body. Because of their critical importance, RF coil technologies have seen tremendous progresses over the past 40 years. The geometry has evolved from volume transmit/receive coils to phased array coils, the frequency tuning has gone from single-tuned to multiple-tuned coils, the number of functions performed by the same coil has increased to include not only signal excitation/reception, but also localized B_0 shimming and wireless data transmission, just to name a few examples. Given the breadth and depth of the RF coil technology evolution, it is simply not possible to review all the exciting innovations in this review article. Rather, we narrow our focus to the past 5 years, while noting that none of these recent advances would have been possible without the solid foundation from early works. For example, the recent integrated RF/shim coils are built on the technical foundation of multiple-tuned RF coils. For a general review of the fundamental principles of RF coils, see Ref. 1.

What is remarkable is that even after four decades of continuous development, the progress of RF coil technology has not shown any signs of slowing down. On the contrary, the pace of innovations has increased over the recent years, resulting in the emergence and increased popularity of flexible RF coil arrays, wireless RF coil arrays, and integrated RF/shim coil arrays. In this review, we discuss the theories, implementations, promising results including commercial adoptions, as well as future outlooks related to recent advances in these three categories of coil arrays, which we hope will provide readers a glimpse of the exciting state of the RF coil technology development.

Flexible RF Coil Arrays

Modern clinical RF receive phased arrays, with a large number of standard copper coil elements[2–4] used for highly accelerated parallel imaging,[5–7] are housed within (semi-)rigid enclosures that provide structural stability and prevent damage to coil elements from patients (Fig. 1). The enclosures also allow the coil elements to be precisely positioned at a fixed location in an array so that the correct coil overlap between adjacent coil elements, referred to as the critical overlap, is used to minimize the mutual inductance (eg, RF coupling) between them, which would otherwise decrease the signal-to-noise ratio (SNR) in the image.[8–10] For example, circular coil elements used in many arrays require a coil overlap of ~25% of their diameter to minimize the RF coupling between them.[10] However, while rigid enclosures allow the coil element positions to be optimized, they can also: increase patient discomfort, potentially causing motion artifacts in the images; and prevent the coil elements from being placed next to the patient's anatomy, which can reduce the SNR in nearby regions. Further, rigid coil arrays limit the ability to perform studies of flexible high-mobility patient anatomy (eg, musculoskeletal (MSK) joint soft tissue), which requires the coil elements to be placed close to the patient to evaluate complex joint motion.[11,12] To address these limitations, new flexible coil array designs have been proposed based on new coil design concepts, conductor technologies, and manufacturing techniques to comfortably conform the coil elements to the patient's anatomy and to provide high-quality diagnostic images.

Flexible Transmission Line Resonator RF Coil Arrays

The flexibility of standard coil elements is physically limited by the electric components (eg, capacitors, diodes, inductors, preamplifiers) on the printed circuit boards and by the lumped capacitors that are placed about the perimeter of the coil elements to tune them to the Larmor frequency and to evenly distribute the received RF currents on the coil conductors for a more uniform image SNR. The capacitors on the coil conductors are soldered in place and are prone to crack under patient load or any bending of the coil elements, which limits both their flexibility and reliability. These risks are more prevalent for coil arrays with a large number of coil elements or used in ultra-high field applications (eg, 7T), both of which have an increased number of lumped components in the array.

In contrast, a monolithic transmission line resonator (TLR) coil design can be made to be flexible and requires no lumped capacitors on the coil conductors because it instead uses two gapped conductors separated by a dielectric substrate (Fig. 2a), which provides the inductance (i.e., conductor trace width and length) and capacitance (i.e., conductors separated by the dielectric substrate) to tune the coil and distribute the RF currents.[14,15] The use of distributed components instead of lumped components makes TLR coils much more flexible so that they can conform to the patient's anatomy to achieve a higher SNR. Preliminary phantom results showed that a flexible TLR coil element provided a 20% increase in SNR and a similar B^{+}_{1} field compared to a standard coil element.[15]

To create a TLR coil array, new techniques must be used to decouple the coil elements from one another because methods that require a precise coil overlap, namely lumped components or additional conductive layers to provide isolation between the coil elements,[16,17] are not suitable for this design. Instead, RF decoupling is provided by adding coil annexes to the top and bottom conductors in the design and then directly overlapping the top and bottom annexes from adjacent coil elements to cancel the mutual inductance between them (Fig. 2a). For example, a flexible four-channel dual gap TLR annexed coil array built on a Teflon substrate (Fig. 2b) had more than −14 dB of isolation between coil elements from the annexes and was able to acquire images of a flat or curved phantom with a similar SNR and image quality (Fig. 2c). The annexes provide sufficient RF-isolation for imaging, but limit the placement of the coil elements in the array and have suboptimal sensitivity profiles for parallel imaging. An alternative decoupling technique uses "decoupling rings" about the perimeter of specific coil elements instead of annexes to provide isolation between coil elements,[18] which allows them to be placed more freely in a TLR coil array and to provide more uniform sensitivity profiles. However, TLR coil arrays provide a less uniform image SNR and sensitivity profiles for parallel imaging relative to coil arrays in which all the coil elements are overlapped with no spaces between them (eg, rigid soccer-ball coil array).[19] Nevertheless, they still remain a viable future technology for specific imaging applications that require a flexible coil array for improved image quality.

Flexible Screen-Printed RF Coil Arrays

Although flexible, the TLR coil design uses standard copper conductors for its coil elements, which ultimately limits the flexibility due to stress cracks that develop when they are made to conform tightly to a patient. Previously, coil conductors filled with mercury[20,21]

or braided copper conductors[22] have been used to improve the flexibility, which allowed the coil to conform to the patient but created safety concerns or produced a suboptimal image SNR. More recently, the design and manufacturing of flexible coil conductors have evolved to include elastomer-based materials[23] and silver conductors woven into fabric[24] that are highly stretchable and mechanically robust, while maintaining adequate electrical performance and improving manufacturing ease. One promising recent direction integrates modern printing techniques to construct inkjet-printed conductors[25] and rapid-production screen-printed coil (SPC) conductors, which are created by depositing multiple layers of special conductive and dielectric inks[26] onto a highly flexible plastic film that can conform to the subject. Interestingly, the screen-printing process also allows the usual lumped capacitors used on standard coils to be replaced with embedded distributed capacitors by changing the relative thickness of the conductive and dielectric inks at the desired capacitor locations around the perimeter of the coil element conductor. Like in the TLR coil design, the distributed capacitors on the coil elements significantly improve the flexibility and reliability of the array, but the SPC design still requires the same critical overlap as a standard coil array,[8] which restricts the layout of the coil elements in coil arrays with complex geometries.

So far, the SPC array technology has been used for both brain,[27] and pediatric imaging,[28] which is a natural clinical application for SPC arrays because they can be printed on a blanket-like material to provide comfort while positioning the coil elements close to the subject. In the latter study, a 12-channel pediatric SPC array was constructed and evaluated for its feasibility, image quality, and caregiver acceptance by imaging 20 pediatric subjects and comparing the results to those of a 32-channel standard coil array. The coil arrays were reported to have a similar average SNR in the paraspinal, abdominal wall, and psoas muscles, but the SPC array had a better g-factor for parallel imaging because its flexibility provided more coil elements in the field-of-view (FOV). Further, a radiologist scored all 20 cases imaged with the SPC array as diagnostically acceptable and found them comparable to those imaged with the ill-fitting 32-channel coil array despite it having 20 more coil elements. Finally, surveyed caregivers (i.e., technologists, anesthesiologists, nurses, parents) and subjects overall favored the comfortable SPC array. In the future, development of better cable management, input baluns, and the ability to rapidly design and manufacture coil arrays with optimized coil placements to provide the highest SNR should make SPC arrays an interesting alternative for imaging.

Highly Flexible RF Coil Arrays

Recently, novel highly flexible lightweight coil designs that can conform to the patient, require no lumped components, and have a broad critical overlap region have been proposed, which allows the coil elements to be placed more freely in the array to achieve a higher SNR and improve the image quality. For example, the proof-of-concept high-impedance coil (HIC) design uses a high-impedance flexible coaxial coil conductor, an LC circuit, and a standard MRI preamplifier to simultaneously acquire the RF signal voltage and provide RF-isolation between coil elements. This unique high-impedance design provides isolation by eliminating all induced RF currents when the impedance is lower at the port than at the coil, which provides a comparatively large critical overlap region compared to that of

standard coil arrays (Fig. 3a), so that coil elements can be placed more freely in an array to optimize the geometry for, as an example, parallel imaging.[11,29] Similar to the TLR and SPC designs, the HIC design uses no lumped components on the coil conductor and has the additional advantage of using the electrical and mechanical properties (eg, substrate permittivity, ratio of coaxial conductor diameters, length) of the flexible coax to tune the coil to resonate at the Larmor frequency instead of lumped components in a matching circuit, which further reduces the number of components in the coil. Additionally, the flexible coax conductor can conform to patients without damage and is only limited by the coax bend-radius, which is beneficial for high-mobility imaging applications such as knee and wrist imaging.

To illustrate the benefits of the HIC design, proof-of-concept MRI experiments were conducted with an eight-channel HIC glove array: to show that images acquired with this array had a comparable SNR and image quality as those acquired with a form-fitting standard 16-channel wrist coil array; and to demonstrate the flexibility of the HIC design during imaging. Specifically, T_1-weighted turbo spin echo (TSE) images of a human wrist were acquired on a 3T scanner with both the eight-channel HIC glove array and the 16-channel rigid coil array, which showed that the average SNR of the HIC array improved near the fingers by 80% and only decreased by 3% over the entire FOV (hand + wrist) despite having half the number of coil elements (Fig. 3b). In another experiment, a separate set of T_1-weighted TSE images were acquired with the HIC glove array while a subject moved their hand from a flat position in the scanner to tightly holding a peach, all while imaging. Remarkably, these images showed minimal change in SNR or image quality for the same anatomical regions (eg, fingers) between the two drastically different coil positions and the HIC array was able to image the motion of the wrist between them, which highlights both the flexibility and possible new research opportunities associated with the HIC design (Fig. 3c). However, this design still has technical challenges that need to be addressed before a widespread adoption of the technology is clinically possible. For example, imaging applications that use coil arrays with large coil elements (eg, body imaging) would require HIC coil elements to have an extremely thick dielectric substrate for tuning, which would significantly decrease the flexibility of the array. Still, the large critical overlap region and high flexibility of the HIC design have shown that it is a potential future technology that can be used for a variety of imaging applications and provide new MRI research opportunities in high-mobility anatomical regions.

A second highly flexible and commercially available design, termed the adaptive image receive (AIR) coil (GE Healthcare, Waukesha, WI), that can conform to the patient and requires no lumped components on the coil conductor has been developed to provide ultra-lightweight coil arrays with an optimized geometry for parallel imaging applications in the clinic. The AIR coil array geometry can be optimized because, like in the HIC design, the coil elements have a large critical overlap region provided by the combination of a proprietary extremely thin coil conductor (i.e., INCA wire) and on-board electronics (i.e., “E-mode” preamplifier), which allows them to be placed freely in an array to achieve a high SNR and improved image quality relative to similar standard coil arrays.[30] These coil attributes allow the AIR coil design to be used in extremely flexible configurations, such as a pediatric coil array embedded in foldable cloth materials.

The AIR coil design was evaluated in vivo for head and neck, MSK, and pediatric imaging. For head and neck imaging, T_2-weighted images of a healthy volunteer were acquired using parallel imaging on a 3T scanner with both a 16-channel AIR coil array (Fig. 4a) and a 30-channel standard head and neck coil array (Fig. 4b) in the same session, but with repositioning of the subject between scans with the different arrays.[12] The study showed that the AIR coil array, which was constructed of four "paddles" each containing four AIR coil elements, provided a qualitatively similar image quality as that of the standard coil array (Fig. 4c,d), despite having significantly fewer coil elements because the overlap between coil elements could be adjusted freely (0–30 mm), which allowed them to be placed close to the subject to achieve a high SNR. The AIR coil design was also used to image the ankle of a healthy volunteer to demonstrate its ability to image high-mobility regions of the body,[31] similarly to the HIC design. The 15-channel MSK AIR coil array used in this study provided a higher SNR in the ankle and lower leg than a standard eight-channel coil array because it could flexibly conform to the patient's anatomy, although it did have more coil elements. Finally, multiple AIR coil blanket arrays were used for pediatric imaging in the chest, abdomen, pelvis, and extremities to evaluate their flexibility and diagnostic image quality in the clinic.[12] In this study, acceptance testing performed on MR technologists, nurses, and medical doctors showed that doctors and nurses all preferred the flexible AIR coil arrays compared to standard coil arrays, while only 4% of technologists preferred the standard coil arrays. Further, all of the cases were found to be of diagnostic quality within an 85% confidence interval.

Wireless RF Coil Arrays

Most clinical RF coil arrays currently require large bulky cable assemblies to connect to the scanner, along with additional RF components (eg, baluns, cable traps) to ensure patient safety and to maintain image quality. For modern arrays with a large number of coil elements designed to improve SNR and achieve highly accelerated imaging,[1,2,32] the cable assemblies become hard to manage, which can increase patient discomfort and setup times, and reduce patient throughput. Further, the cable assemblies used by many of the highly flexible lightweight coil arrays are the heaviest component in the array and present the biggest obstacle to achieve a comfortable, unrestricted design. Additionally, the cable assemblies of peripheral devices used, for example, for physiological monitoring of patients (eg, respiratory motion) require careful routing in the scanner and can present the same aforementioned issues. To eliminate the cable assemblies from these coil arrays and peripheral devices, wireless technologies must be integrated into them to wirelessly transmit the MRI or peripheral data outside of the scanner bore without degrading image quality or requiring significant modifications to the scanner. Indeed, some of the early advances have already been adopted by major MR manufacturers (eg, Siemens, GE, and Philips) and third-party companies for patient monitoring devices (eg, Invivo).

Wireless RF Coil Arrays for Wireless MRI Data Transfer

A truly wireless coil array with no wired connections to the MRI scanner requires wireless data conversion and synchronization, wireless data transfer, and a wireless power source for all the electronics needed to acquire and transmit the data. The analog MRI RF signal

acquired from the subject must first be sampled, digitized, and potentially compressed for large data sets (eg, from arrays with many coil elements) before it can be wirelessly transmitted. To this end, the analog RF signal can be sampled "on-coil" with high-speed, high-resolution, MR-compatible analog-to-digital converters (ADCs) using analog down conversion,[33] direct undersampling,[34,35] or baseband demodulation sampling techniques,[36] which can reduce the amount of data, and therefore the data rate, to be wirelessly transmitted.[37] For example, a modern 3T 64-channel RF coil array has been estimated to only require a minimum data rate of 512 Mbps, or 8 Mbps/coil element, using 16-bit ADCs and a demodulated baseband technique.[33,38,39] Critically, the ADCs data acquisition clock must be wirelessly synchronized with the MRI scanner clock using additional software and in-bore hardware to avoid clock-jitter, which effectively reduces the number of ADC sampled bits and can result in image artifacts.[40,41] The clock synchronization is an active area of research in wireless MRI and is a major obstacle to the ubiquitous use of wireless MRI in a clinical setting.

Previously proposed methods to wirelessly transmit properly sampled and synchronized MRI data from the RF coil to the scanner electronics have used two main wireless radiation mechanisms: near-field inductive coupling and far-field wireless data transmission. Inductively coupled transmission allows the analog signal to be wirelessly transferred between two or more additional coils placed in the scanner bore,[42] which has no data rate transmission requirements because the signal is not digitized in-bore. Further, this method of data transfer uses minimal electronics to sever the cable connection in the bore but requires careful setup[43,44] and can decrease SNR,[45] which reduces patient throughput and image quality. The alternative far-field methods for wireless MRI have mostly used additional 2.4- or 5-GHz WiFi (eg, 802.11 b/g/n/a/c)[46] and WiGig 60-GHz (eg, 802.11 ad) (Fig. 5) antennas and low-power electronics[38,39,47] to wirelessly transfer data in the scanner bore, which can reliably provide data rates between 11 Mbps (802.11b) and 500 Mbps (802.11 ad) with low bit-error.[38] Excitingly, proof-of-concept MRI experiments have first been conducted to wirelessly transfer data at low data rates (eg, <100 Mbps)[48,49] and more recently with WiGig at high data rates (eg, >100 Mbps) suitable for RF coil array applications[47] (Fig. 5b), which demonstrated the ability of these methods to wirelessly transmit data in the bore without decreasing the image SNR. These systems do not require any expensive scanner bore modifications and can easily be used with existing scanners; however, they require an additional antenna system in the bore for some low data rate[46] and the WiGig high data rate wireless data transfers. In practice, high-frequency antenna designs are generally susceptible to higher radiated losses in tissues, result in a higher specific absorption rate (SAR) in subjects, and use highly directional antennas to transfer data, which therefore must be placed carefully within the bore to minimize losses and SAR in the subject, optimize data transfer, and avoid coupling when placed near other electronics (eg, RF coil array, scanner wiring). Still, these antenna systems can be designed and optimized for use in the scanner, which can help improve the implementation of wireless RF coil arrays in MRI.[50] Lastly, we note that wireless systems that can transfer data at low and high data rates both have potential in MRI as each is highly dependent upon the RF coil array application. For example, an extremely high data rate system is required for high-density neuroimaging coil arrays,[1,2] but a lower

data rate system with cheaper electronics would be suitable for a four-channel cardiorenal coil array[51] or the aforementioned eight-channel HIC glove array.

All of these wireless technologies for RF coil arrays require alternative power sources for their on-board electronics (eg, processors, ADCs, and wireless transceivers), which can have power requirements between an estimated 10 and 100 W for high-density coil arrays.[33] Innovatively, the MRI scanner itself can be used to provide power to the electronics by using two or more additional coils in the scanner to harvest power from the scanner RF transmit pulses during imaging. Specifically, this wireless power transfer (WPT) system uses a secondary coil tuned to the Larmor frequency to gather energy from the high-power scanner RF transmit pulses (eg, 10–30 kW) and to inductively couple it to a primary coil, where it can then be rectified and used to power electronics[52–55] (Fig. 5c). These systems have shown the ability to harvest up to 13 W from a 1.5T scanner, which is sufficient to power, for example, the 60-GHz wireless transceivers for any modern high-density coil array.[38] A challenge for the WPT system is that it must be precisely positioned in the scanner bore to prevent it from coupling with the RF coil array and decreasing image SNR, which suggests that it must be integrated into the scanner. While a significant and costly implementation for existing scanners, a fully integrated WPT system in future scanners could provide a possible power solution for wireless electronics in the bore. For more information, an extensive review of wireless RF coil array hardware is presented in Ref. 33.

Wireless RF Coil Arrays for Wireless Data Transfer from Peripheral Devices

In MRI, peripheral devices are used to monitor patient physiological motion (eg, pulse oximeter, respiratory belt, motion sensor) or spatiotemporal changes in the magnetic field (eg, field cameras) to correct for subject- or system-related artifacts. In the past, these devices required wired connections from inside the scanner bore to power supplies and computers in the machine or console rooms. Recently, and similarly to the wireless RF coil arrays mentioned above, these wired connections are gradually being replaced by wireless products to increase patient comfort, safety, and throughput.

Rigid-body motion can be wirelessly detected by adding small inductively coupled coils near the subject and by identifying changes in the MRI signal frequencies when gradients are applied in the imaging pulse sequence.[56–58] These changes in frequencies allow the positions of the coils and hence the amount of subject movement during the scan to be determined, which can then be used to correct for motion artifacts in the images. In another innovative wireless rigid-body motion detection system, short-wave RF signals are transmitted to passive sensors placed on the subject and the reflected RF signals are then measured to determine the subject's position.[59] By removing wired connections, these sensors decrease the risk of local heating to the subjects and the time required to set up the motion detection systems.

Additionally, cardiac and respiratory motion during MR image acquisition can generate artifacts in the images that significantly reduce their clinical diagnostic quality. To correct for such artifacts and improve the image quality, many solutions have been proposed, including pulse sequence gating techniques,[60–63] camera systems,[64–66] fiber-optic sensors,[67] and novel ultrasound (US) based organ configuration motion (OCM) sensors.[68–70] The

unique OCM sensor attaches to the skin and can characterize the internal movement of organs during cardiac and respiratory motion (Fig. 6a), which provides significantly more anatomical information compared to, for example, respiratory bellows. However, each of these hardware systems currently use wired connections to power the devices and to transmit data outside of the scanner room. As such, they require additional technologies to provide wireless data transfer for the sensors.

Most peripheral devices, as adopted by industries thus far, are made wireless by using additional antenna systems and electronics in the scanner bore to transmit sensor data outside of the scanner room, which has the same aforementioned disadvantages as for RF coil arrays. Alternatively, a new integrated RF/wireless (iRFW) coil design[48] can be used to simultaneously acquire MR images and wirelessly transmit sensor data outside of the scanner bore by allowing RF currents both at the Larmor frequency (eg, 127.7 MHz for a 3T scanner) and within a wireless communication band (eg, 2.4 GHz for WiFi) to flow on the conductors of the same coil element (Fig. 6b), which eliminates the need for additional antenna systems in the scanner bore.[71] A conventional RF coil element can be modified into an iRFW coil element by adding high-impedance bandstop filters at the Larmor or wireless frequencies between the coil element and the wireless module or the MRI preamplifier, respectively, to prevent RF losses incurred to both of them in their respective frequency bands. Proof-of-concept phantom experiments with an iRFW coil showed its ability to simultaneously acquire MR images and wirelessly transmit US data acquired with a 1-MHz OCM sensor to a computer in the console room with no degradation in image SNR (Fig. 6c) or US data quality (Fig. 6d).[72] The US data were digitized and modulated in-bore using a battery-powered MR-compatible custom ADC printed circuit board and modified Raspberry Pi Zero (~100 mW), respectively. Notably, for this and other low-power applications,[36,67] MR-compatible batteries that are commercially available are an easy and viable option to provide power to in-bore electronics. With this design, the RF coil array eliminates the need for any additional antenna systems by simply changing the electrical design of one or more coil element(s) in the array and the in-bore electronics can be miniaturized to save space in the scanner bore. The iRFW coil design thus provides an in-bore wireless hub for the wireless transmission of data from peripheral devices.

Integrated RF/Shim Coil Arrays

Magnetic susceptibility differences at air/tissue interfaces induce static magnetic field inhomogeneities (ΔB_0) in many regions of the human body, including the inferior frontal and temporal brain regions, spinal cord, breast, and abdomen. These localized B_0 inhomogeneities can result in image artifacts (eg, geometric distortions in echo-planar imaging (EPI), blurring in non-Cartesian imaging, signal loss in gradient-echo imaging), increase spectral line widths in MR spectroscopy, and reduce the effectiveness of fat saturation, water-fat separation, and water suppression.[73] All of these issues limit the diagnostic accuracy and prevent a wider clinical application of valuable MRI techniques such as diffusion-weighted imaging (DWI).

The most common B_0 shimming method, which is spherical harmonic (SH) shimming,[74] consists in approximating the B_0 inhomogeneities to be shimmed with a sum of orthogonal

SH terms up to a certain order. Each of these terms can then be canceled by generating a corresponding ΔB_0 field with an opposite polarity. Specifically, a global B_0 offset (zeroth-order term), linear B_0 gradients (first-order terms), and higher-order ΔB_0 fields (second-order terms and above) are generated by adjusting the resonance frequency, by using the $x/y/z$ gradient coils, and by using additional whole-body SH shim coils embedded in the scanner bore, respectively. While higher-order SH shim coils can provide a more effective shimming, they also require additional space within the scanner bore and expensive shim current supplies. Thus, SH shimming is typically limited to the second order on most scanners and cannot effectively shim localized B_0 inhomogeneities. Multi-coil shimming,[75,76] which uses an array of smaller localized shim coils placed closer to the body, was shown to be more effective than second- or third-order SH shimming, but the localized shim coil array competes with the RF coil array for the same space near the body and must be placed inside or outside the RF coil array, which can result in a suboptimal SNR or shimming performance.

To address these limitations, integrated RF/shim coil designs[77–79] have recently been proposed, in which RF currents at the Larmor frequency and direct currents (DC) can both flow on the same coil elements, thereby enabling RF excitation/reception and localized B_0 shimming, respectively, with a single coil array rather than two separate RF and shim coil arrays. Integrated RF/shim coils are also referred to as integrated parallel reception, excitation, and shimming (iPRES) coils, integrated ΔB_0/Rx coils, or AC/DC coils. While most designs are only used for RF reception and B_0 shimming, some of them can additionally be used for RF excitation.[77,80,81]

A conventional RF coil array can be relatively easily modified into an integrated RF/shim coil array by adding (Fig. 7a): a multi-channel DC power supply to provide an adjustable DC current to each coil element; a shielded twisted-pair DC cable with chokes to provide RF-isolation between the power supply and each coil element; and inductors to bypass the capacitors and allow a DC current to flow on each coil element.[78,79] Shimming with integrated RF/shim coil arrays is performed by: acquiring a set of basis ΔB_0 maps on a phantom with a known DC current applied in one coil element at a time (which only needs to be done once); acquiring a baseline ΔB_0 map in the subject; and determining the optimal DC currents to apply in all coil elements to minimize the B_0 inhomogeneity in the volume or slice of interest (which is typically calculated as the root-mean-square error between the baseline ΔB_0 map and a linear combination of the basis ΔB_0 maps), subject to a maximum current constraint.[82]

The shimming performance of integrated RF/shim coil arrays in the human brain was shown to be superior to that of second-order SH shimming and comparable to that of higher-order SH shimming or multi-coil shimming (Fig. 8a).[73,78,79] Importantly, most implementations of integrated RF/shim coil arrays do not degrade the SNR.[71,78,82–84] Thus, integrating an RF coil array and a localized shim coil array into a single RF/shim coil array enables both a high RF and shimming performance to be achieved without requiring additional space within the scanner bore. Additionally, the low inductance of the coil elements allows the DC currents to be quickly updated to dynamically shim individual slices in a multi-slice acquisition (or

groups of slices in a multi-band acquisition), resulting in a more effective shimming than global (eg, whole-brain) shimming.[73,87,88]

One potential limitation of integrated RF/shim coil arrays is that the coil geometry (i.e., number, size, shape, and location of the coil elements) may not always be optimal to achieve both a high RF and shimming performance. For example, the coil elements of a body coil array, which are typically larger than those of a head coil array, may not be sufficiently small to shim the localized B_0 inhomogeneities in the abdomen. To address this issue, the iPRES(N) coil design[82] was proposed, in which each RF coil element is split into N smaller RF-isolated DC loops, each with an independent DC current (Fig. 7b), resulting in a larger number of more localized ΔB_0 fields available for shimming and hence in a more effective shimming of localized B_0 inhomogeneities compared to the original iPRES(1) coil design.[82,83] One drawback of the iPRES(N) coil design, however, is that it requires an N-fold increase in the number of DC power supplies and in the associated cost. In the adaptive iPRES (N) coil design,[89,90] microelectromechanical system switches are used to direct the DC current from a single DC power supply per RF coil element into the appropriate DC loops as needed for shimming (Fig. 7c), providing a comparable shimming performance as that of an equivalent iPRES(N) coil design, but without requiring additional power supplies. Other approaches to improve the shimming performance of integrated RF/shim coil arrays consist in adding DC loops that are only used for shimming and are either located in regions not covered by RF/shim coil elements, such as over the face (Fig. 7d,e),[73,91] or placed orthogonal to some of the RF/shim coil elements (Fig. 7f), although at the expense of occupying more space in the scanner bore.[92]

The iPRES and iRFW (see previous section) coil designs can also be combined to allow RF currents both at the Larmor frequency and within a wireless communication band as well as a DC current to flow on the same coil element (Fig. 7g), thereby enabling MR imaging, wireless communication, and localized B_0 shimming, respectively, with a single coil element.[48] This wireless iPRES (iPRES-W) coil design thus enables wireless localized B_0 shimming using DC currents that are supplied by an MR-compatible battery pack within the scanner bore and wirelessly controlled by a computer located outside the scanner room.[84] In the dual-stream iPRES-W coil design, two iPRES-W coil elements (along with additional iPRES coil elements) are used to enable two concurrent wireless applications, such as wireless localized B_0 shimming and wireless respiratory monitoring with a respiratory belt.[71]

While still relatively recent, integrated RF/shim coil arrays have already been used to shim localized B_0 inhomogeneities in multiple applications in the human brain,[71,73,78,79,85–88,93] abdomen,[82,89,90] spinal cord,[84,94,95] and breast,[83] as well as the monkey brain[96] and rat brain.[97] Specifically, they have been used: to correct for geometric distortions in EPI (Fig. 8b,d),[71,73,78,79] including for DWI (Fig. 8f),[83,90] diffusion tensor imaging (DTI) (Fig. 8e),[84,87,88] and quantitative parameter mapping[93]; to recover signal loss in gradient-echo EPI for fMRI (Fig. 8c) using a new cost function in the shim optimization that directly accounts for the signal loss[86]; to dynamically shim respiration-induced ΔB_0 changes in real time using a respiratory sensor[95]; and to reduce spectral line widths and improve metabolite

quantification in MR spectroscopic imaging (MRSI) (Fig. 8g), including in patients with brain tumors.[85]

While integrated RF/shim coil arrays were originally designed for B_0 shimming, their ability to precisely and quickly control the ΔB_0 field in space and time has more recently also been exploited for many other applications. For example, spatially selective excitation can be achieved without requiring specialized pulse sequences by applying a tailored nonlinear ΔB_0 pattern during the RF excitation, so that only the spins in the target region-of-interest (ROI) are on resonance while those outside the ROI are not, thereby enabling zoomed three-dimensional (3D) EPI in the visual cortex with a reduced FOV or in the peripheral cerebrum with a higher undersampling and reduced g-factor penalty (Fig. 9a).[98] Lipid suppression in MRSI can be improved by applying a tailored ΔB_0 offset during the lipid suppression RF pulse, so that the water and lipid peaks are further separated in the frequency domain, resulting in reduced chemical shift artifacts (Fig. 9b).[99] Cerebral blood flow territory mapping can be performed with arterial spin labeling (ASL) by controlling the ΔB_0 field near specific arteries in the labeling plane during the labeling RF pulses, so that only the spins in the artery of interest are on resonance and are labeled, while those in other arteries are shifted outside the passband of the labeling pulses (Fig. 9c).[100] A more uniform B_1^+ field and flip angle distribution can be achieved at 7T without requiring parallel transmission by jointly optimizing the RF waveform from a birdcage transmit coil, the $x/y/z$ gradient waveforms, and the shim waveforms from an integrated RF/shim coil array, which provides additional degrees of freedom to perform spatially varying spin dephasing during the RF pulse (Fig. 9d).[101] The precision and efficiency of MR fingerprinting can be improved by adding spatiotemporal ΔB_0 (and even B_1^+) variations throughout the pulse sequence in addition to the traditional variations in flip angle and repetition time, thereby improving the encoding capabilities of MR fingerprinting, the uniqueness of the signal evolutions from different tissues (i.e., the “fingerprints”), and the ability to identify the underlying tissue properties using pattern recognition of these fingerprints (Fig. 9e).[80,102] Finally, wave-encoding parallel imaging, which applies a low-frequency wave-encoding of the gradient waveforms during the data acquisition to achieve high accelerations with minimal g-factor penalty, can be further accelerated (up to ~20-fold) by adding a high-frequency wave-encoding of the shim waveforms from an integrated RF/shim coil array (Fig. 9f).[103] While some of these results are still preliminary, all of these examples nevertheless illustrate the usefulness, versatility, and potential of integrated RF/shim coil arrays for a wide range of applications.

Discussion and Outlook

The RF coil technologies are constantly evolving and expanding. Surely, there are new breakthroughs already in development that are not mentioned or adequately discussed in this review article. However, we hope that our highlights provide the readers with a snapshot of some of the recent exciting advances in this dynamic field.

This review would not be complete without providing some prospective discussions on the RF coil development. “After all, the past is our only real guide to the future,” as author Michael Mandelbaum fittingly puts it. So where are the RF coil technologies headed?

Flexible RF Coil Arrays

The highly flexible HIC and AIR coil arrays will clearly have extensive applications in diagnostic imaging but they can also play an important role in therapeutic interventions. These coil designs have a small coil conductor and require no lumped capacitors, which can otherwise have high radiation attenuation factors that can change the dose delivered to the patient during treatment. As such, these RF coil designs are good candidates for use in MR-LINAC (linear accelerator) radiation therapy treatments to provide precise imaging of tumor target volumes without reducing the radiation dose presented to the patient.[12,29] Similarly, these coil arrays can be used in MR-PET clinical applications to identify cancers in the head and neck,[104] prostrate,[105] and thyroid[106] during pretreatment planning. Since these lightweight coil arrays can be sewn into blankets that can be comfortably wrapped around the patient, it is feasible to use a single HIC or AIR coil array that can travel with the patient during pretreatment diagnostic imaging and therapeutic radiation treatments without having to reposition the coil array on the patient to provide a consistent coil coverage of the anatomy.

Wireless RF Coil Arrays

Wireless RF coil designs have already demonstrated the ability to wirelessly transfer MRI data at sufficient data rates for existing high-density coil arrays. In the future, even higher data rates can be expected as the number of coil elements in arrays, the spatial resolution used in many applications, and the size of datasets from peripheral devices (eg, 4K video) all increase, which may require different modulation techniques for wireless data transfer. A possible solution is to use current cellular mmWave 5G multiple-input, multiple-output (MIMO) technologies[107,108] to wirelessly transmit data in the scanner. For example, a 4 × 4 MIMO 28-GHz 5G wireless system has measured uplink and downlink throughput speeds of approximately 1 and 9 Gbps, respectively,[109] which would be sufficient to wirelessly transmit any MRI dataset in the foreseeable future. For this system, the mmWave antennas would clearly have to be optimized for use in the MRI scanner bore, similarly to many of the wireless systems mentioned above. Alternatively, these antennas could be replaced with iRFW coil elements in an array (eg, an iRFW mmWave coil array) to provide an antenna design for an optimal throughput in the scanner bore. Additionally, this system would require WiFi-equivalent 5G in-bore electronics and an access point (eg, 5G router) to enable wireless data transfer between the iRFW coil array and the console room, which are expected to become commercially available, similarly to long-term evolution (LTE) cellular access points that are used in homes today. The combination of extremely high throughput wireless technologies and highly flexible coil arrays will significantly change the patient interaction with the MRI scanner environment. For example, pediatric imaging with a high-throughput wireless flexible blanket coil array used with “quiet” MRI pulse sequences[110] would allow pediatric patients to rest comfortably while swaddled in the array with no wired connections to the scanner, which would permit the MR technologist to position them in a way that provides the best images.

Integrated RF/Shim Coil Arrays

As discussed earlier, the ability of integrated RF/shim coil arrays to simultaneously acquire MR images and shim localized B_0 inhomogeneities has been demonstrated in brain imaging for multiple applications, including DTI, fMRI, MRSI, and quantitative parameter mapping. Moreover, they have also shown promising results in abdominal, spine, breast, and animal imaging, as well as for nonshimming applications such as spatially selective excitation, lipid suppression, cerebral blood flow territory mapping, flip angle uniformization, MR fingerprinting, and wave-encoding parallel imaging. While some of these more recent applications are still under development, the unique ability of integrated RF/shim coil arrays to control the ΔB_0 field in space and time without requiring additional space in the scanner bore or degrading the SNR is expected to benefit a growing number of research and clinical applications.

Along those lines, another function that could potentially be performed by integrated RF/shim coil arrays is spatial encoding. Traditionally, spatial encoding is achieved by using gradient coils. However, since integrated RF/shim coil arrays can already generate individual ΔB_0 fields for shimming, the same ΔB_0 fields can in principle also be used for spatial encoding. Not surprisingly, there have been recent reports on using localized shim coil arrays to perform both linear[111] and nonlinear[112] spatial encoding, and promising preliminary results have shown the ability of these methods to resolve spatial details. However, performing spatial encoding with the single-turn coil elements of integrated RF/shim coil arrays rather than the multi-turn coil elements of multi-coil shim arrays remains technically challenging, as the ΔB_0 fields and hence DC currents needed to generate sufficiently strong gradients for spatial encoding can be much greater than those used for shimming. As such, power and heating issues for this new application of integrated RF/shim coil arrays need to be carefully managed.

Final Thought

One radical idea, integrating all the RF coil advances discussed in this review, is an ultra-light flexible, wearable, and self-powered RF head coil helmet that can perform RF excitation/reception, spatial encoding, localized B_0 shimming, and wireless transfer of the MR signal and other signals from peripheral devices to the scanner console. Imagine that for our future. This seems like a good place to end.

Acknowledgments

This study received grant support from NIH (R01 NS075017, R01 EB028644) and GE Healthcare.

References

1. Gruber B, Froeling M, Leiner T, Klomp DWJ. RF coils: A practical guide for nonphysicists. J Magn Reson Imaging 2018;48:590–604. [PubMed: 29897651]
2. Wiggins G, Polimeni J, Potthast A, Schmitt M, Alagappan V, Wald L. 96-Channel receive-only head coil for 3 Tesla: Design optimization and evaluation. Magn Reson Med 2009;62:754–762. [PubMed: 19623621]
3. Schmitt M, Potthast A, Sosnovik DE, et al. A 128-channel receive-only cardiac coil for highly accelerated cardiac MRI at 3 tesla. Magn Reson Med 2008;59:1431–1439. [PubMed: 18506789]

4. Fujita H, Zheng T, Yang X, Finnerty MJ, Handa S. RF surface receive array coils: The art of an LC circuit. J Magn Reson Imaging 2013;38: 12–25. [PubMed: 23649497]
5. Pruessmann KP, Weiger M, Scheidegger MB, Boesiger P. SENSE: Sensitivity encoding for fast MRI. Magn Reson Med 1999;42:952–962. [PubMed: 10542355]
6. Deshmane A, Gulani V, Griswold MA, Seiberlich N. Parallel MR imaging. J Magn Reson Imaging 2012;36:55–72. [PubMed: 22696125]
7. Larkman DJ, Nunes RG. Parallel magnetic resonance imaging. Phys Med Biol 2007;52:R15–R55. [PubMed: 17374908]
8. Wiggins GC, Triantafyllou C, Potthast A, Reykowski A, Nittka M, Wald LL. 32-Channel 3 tesla receive-only phased-array head coil with soccer-ball element geometry. Magn Reson Med 2006;56:216–223. [PubMed: 16767762]
9. Zhang T, Grafendorfer T, Cheng J, et al. A semi-flexible 64-channel receive-only phased array for pediatric body MRI at 3T. Magn Reson Med 2016;76:1015–1021. [PubMed: 26418283]
10. Roemer PB, Edelstein WA, Hayes CE, Souza SP, Mueller OM. The NMR phased array. Magn Reson Med 1990;16:192–225. [PubMed: 2266841]
11. Zhang B, Sodickson DK, Cloos MA. A high-impedance detector-array glove for magnetic resonance imaging of the hand. Nat Biomed Eng 2018;2:570–577. [PubMed: 30854251]
12. McGee KP, Stormont RS, Lindsay SA, et al. Characterization and evaluation of a flexible MRI receive coil array for radiation therapy MR treatment planning using highly decoupled RF circuits. Phys Med Biol 2018;63:08NT02.
13. Kriegl R, Ginefri JC, Poirier-Quinot M, et al. Novel inductive decoupling technique for flexible transceiver arrays of monolithic transmission line resonators. Magn Reson Med 2015;73:1669–1681. [PubMed: 24753115]
14. Serfaty S, Haziza N, Darrasse L, Kan S. Multiturn split-conductor transmission-line resonator. Magn Reson Med 1997;38:687–698. [PubMed: 9324337]
15. Frass-Kriegl R, Laistler E, Hosseinnezhadian S, et al. Multi-turn multi-gap transmission line resonators—Concept, design and first implementation at 4.7 T and 7 T. J Magn Reson 2016;273:65–72. [PubMed: 27750073]
16. Avdievich NI, Hetherington HP. 4 T actively detuneable double-tuned 1H/31P head volume coil and four-channel 31P phased array for human brain spectroscopy. J Magn Reson 2007;186:341–346. [PubMed: 17379554]
17. Constantinides C, Angeli S. Elimination of mutual inductance in NMR phased arrays: The paddle design revisited. J Magn Reson 2012;222: 59–67. [PubMed: 22820010]
18. Hosseinnezhadian S, Frass-Kriegl R, Goluch-Roat S, et al. A flexible 12-channel transceiver array of transmission line resonators for 7 T MRI. J Magn Reson 2018;296:47–59. [PubMed: 30205313]
19. Zhu Y, Hardy CJ, Sodickson DK, et al. Highly parallel volumetric imaging with a 32-element RF coil array. Magn Reson Med 2004;52: 869–877. [PubMed: 15389961]
20. Rousseau J, Lecouffe P, Marchandise X. A new, fully versatile surface coil for MRI. Magn Reson Imaging 1990;8:517–523. [PubMed: 2392039]
21. Malko JA, McClees EC, Braun IF, Davis PC, Hoffman JC. A flexible mercury-filled surface coil for MR imaging. Am J Neuroradiol 1986;7: 246–247. [PubMed: 3082157]
22. Nordmeyer-Massner JA, De Zanche N, Pruessmann KP. Stretchable coil arrays: Application to knee imaging under varying flexion angles. Magn Reson Med 2012;67:872–879. [PubMed: 22213018]
23. Port A, Luechinger R, Brunner DO, Pruessmann KP. Elastomer coils for wearable MR detection. Magn Reson Med 2021;85(5):2882–2891. [PubMed: 33433044]
24. Vincent J, Rispoli J. Stitching stretchable radiofrequency coils for MRI: A conductive thread and athletic fabric approach. Conf Proc IEEE Eng Med Biol Soc 2019;6798–6801.
25. Mager D, Peter A, Del Tin L, et al. An MRI receiver coil produced by inkjet printing directly on to a flexible substrate. IEEE Trans Med Imaging 2010;29:482–487. [PubMed: 20129848]
26. Krebs FC. Fabrication and processing of polymer solar cells: A review of printing and coating techniques. Sol Energy Mater Sol Cells 2009; 93:394–412.

27. Corea JR, Lechene P, Lustig M, Arias A. Materials and methods for higher performance screen-printed flexible MRI receive coils. Magn Reson Med 2017;78:775–783. [PubMed: 27612330]
28. Winkler SA, Corea J, Lechêne B, et al. Evaluation of a flexible 12-channel screenprinted pediatric MRI coil. Radiology 2019;291: 180–185. [PubMed: 30806599]
29. Zijlema SE, Tijssen RHN, Malkov VN, et al. Design and feasibility of a flexible, on-body, high impedance coil receive array for a 1.5 T MR-linac. Phys Med Biol 2019;64:185004. [PubMed: 31370043]
30. Stormont R, Robb F, Lindsey S, Chu D, Vlachos F. Reimagining flexible coil technology. GE Signa Pulse 2017(Spring);69–71.
31. Collick BD, Behzadnezhad B, Hurley SA, et al. Rapid development of application-specific flexible MRI receive coils. Phys Med Biol 2020;65: 19NT01.
32. Hardy CJ, Giaquinto RO, Piel JE, et al. 128-Channel body MRI with a flexible high-density receiver-coil array. J Magn Reson Imaging 2008; 28:1219–1225. [PubMed: 18972330]
33. Nohava L, Ginefri JC, Willoquet G, Laistler E, Frass-Kriegl R. Perspectives in wireless radio frequency coil development for magnetic resonance imaging. Front Physiol 2020;8(February):1–10.
34. Giovannetti G, Hartwig V, Viti V, et al. Application of undersampling technique for the design of an NMR signals digital receiver. Concepts Magn Reson Part B Magn Reson Eng 2016;46B:41–48.
35. Pérez P, Santos A, Vaquero JJ. Potential use of the undersampling technique in the acquisition of nuclear magnetic resonance signals. Magn Reson Mater Phys Biol Med 2001;13:109–117.
36. Sporrer B, Wu L, Bettini L, et al. A fully integrated dual-channel on-coil CMOS receiver for array coils in 1.5–10.5 T MRI. IEEE Trans Biomed Circuits Syst 2017;11:1245–1255. [PubMed: 29293422]
37. Hashimoto S, Kose K, Haishi T. Comparison of analog and digital transceiver systems for MR imaging. Magn Reson Med Sci 2014;13: 285–291. [PubMed: 25167877]
38. Aggarwal K, Joshi KR, Rajavi Y, et al. A millimeter-wave digital link for wireless MRI. IEEE Trans Med Imaging 2017;36:574–583. [PubMed: 27810803]
39. Vassos C, Robb F, Vasanawala S, Pauly J & Scott G. Characterization of in-bore 802.11ac Wi-Fi performance. In: Proceedings of the 27th International Society of Magnetic Resonance in Medicine. Montreal; 2019;27:1543.
40. Scott G, Vasanawala S, Robb F, Stang P, Pauly J. Pilot tone software synchronization for wireless MRI receivers. In: Proceedings of the 26th International Society of Magnetic Resonance in Medicine. Paris; 2018, 25.
41. Lu JY, Grafendorfer T & Robb F et al. Clock transmission methods for wireless MRI: A study on clock jitter and impact on data sampling. In Proceedings of the 27th International Society of Magnetic Resonance in Medicine. Montreal; 2019;27:1542.
42. Hoult DI, Tomanek B. Use of mutually inductive coupling in probe design. Concepts Magn Reson Part B Magn Reson Eng 2002;15: 262–285.
43. Shchelokova A, Ivanov V, Mikhailovskaya A, et al. Ceramic resonators for targeted clinical magnetic resonance imaging of the breast. Nat Commun 2020;11:1–7. [PubMed: 31911652]
44. Puchnin V, Solomakha G, Nikulin A, Magill AW, Andreychenko A, Shchelokova A. Metamaterial inspired wireless coil for clinical breast imaging. J Magn Reson 2021;322:106877. [PubMed: 33278812]
45. Bulumulla SB, Fiveland E, Park KJ, Foo TK, Hardy CJ. Inductively coupled wireless RF coil arrays. Magn Reson Imaging 2015;33: 351–357. [PubMed: 25523607]
46. Wei J, Liu Z, Chai Z, Yuan J, Lian J, Shen GX. A realization of digital wireless transmission for MRI signals based on 802.11b. J Magn Reson 2007;186:358–363. [PubMed: 17433744]
47. Ko Y, Bi W, Felder J & Shah NJ. Wireless digital data transfer based on WiGig/IEEE 802.11ad with self-shielded antenna gain enhancement for MRI. In: Proceedings of the 27th International Society of Magnetic Resonance in Medicine; 2019;27:1537.
48. Darnell D, Cuthbertson J, Robb F, Song AW, Truong T-K. Integrated radio-frequency/wireless coil design for simultaneous MR image acquisition and wireless communication. Magn Reson Med 2019;81: 2176–2183. [PubMed: 30277273]

49. Cuthbertson JD, Darnell D & Bresticker J et al. The iPRES-W air coil: A flexible RF coil for simultaneous MR image acquisition, wireless communication, and localized B shimming. In: Proceedings of the 26th International Society of Magnetic Resonance in Medicine, Paris, France; 2018;26:16.
50. Bresticker J, Thompson Z, Willey D, Song AW, Darnell D & Truong T-K. Simulations of integrated radio-frequency/wireless coil designs for simultaneous MR image acquisition and wireless communication. In Proceedings of the 27th International Society of Magnetic Resonance in Medicine, Paris, France; 2019;27:1541.
51. Boehmert L, Kuehne A, Waiczies H, et al. Cardiorenal sodium MRI at 7.0 Tesla using a 4/4 channel 1H/23Na radiofrequency antenna array. Magn Reson Med 2019;82:2343–2356. [PubMed: 31257651]
52. Byron K, Robb F, Stang P, Vasanawala S, Pauly J, Scott G. An RF-gated wireless power transfer system for wireless MRI receive arrays. Concepts Magn Reson Part B Magn Reson Eng 2017;47B:1–16.
53. Byron K, Winkler SA, Robb F, Vasanawala S, Pauly J, Scott G. An MRI compatible RF MEMs controlled wireless power transfer system. IEEE Trans Microw Theory Tech 2019;67:1717–1726. [PubMed: 31423023]
54. Venkateswaran M, Kurpad K, Brown JE, Fain S, Van Der Weide D. Wireless power harvesting during MRI. In: Proceedings of the Annual International Conference of the IEEE Engineering in Medicine and Biology Society; 2020, 1469–1472.
55. Moore J, Castellanos S, Xu S, Wood B, Ren H, Tse ZTH. Applications of wireless power transfer in medicine: State-of-the-art reviews. Ann Biomed Eng 2019;47:22–38. [PubMed: 30306381]
56. Sengupta S, Tadanki S, Gore JC, Brian Welch E. Prospective real-time head motion correction using inductively coupled wireless NMR probes. Magn Reson Med 2014;72:971–985. [PubMed: 24243810]
57. Ooi MB, Aksoy M, MacLaren J, Watkins RD, Bammer R. Prospective motion correction using inductively coupled wireless RF coils. Magn Reson Med 2013;70:639–647. [PubMed: 23813444]
58. Godenschweger F, Kagenbein U, Stucht D, et al. Motion correction in MRI of the brain. Phys Med Biol 2016;61:32–56.
59. Schildknecht CM, Brunner DO, Schmid T, Reber J, Marjanovic J & Pruessmann KP. Wireless motion tracking with short-wave radio-frequency. In: Proceedings of the 27th International Society of Magnetic Resonance in Medicine, Montreal, Canada; 2019;27:66.
60. Richter JAJ, Wech T, Weng AM, et al. Free-breathing self-gated 4D lung MRI using wave-CAIPI. Magn Reson Med 2020;84:3223–3233. [PubMed: 32767457]
61. Huang S, Boyacioglu R, Bolding R, Chen Y, Griswold MA. Free-breathing abdominal magnetic resonance fingerprinting using a pilot tone navigator. J Magn Reson Imaging 2021;54:1138–1151. 10.1002/jmri.27673. [PubMed: 33949741]
62. Di Sopra L, Piccini D, Coppo S, Stuber M, Yerly J. An automated approach to fully self-gated free-running cardiac and respiratory motion-resolved 5D whole-heart MRI. Magn Reson Med 2019;82: 2118–2132. [PubMed: 31321816]
63. Rosenzweig S, Scholand N, Holme HCM, Uecker M. Cardiac and respiratory self-gating in radial MRI using an adapted singular spectrum analysis (SSA-FARY). IEEE Trans Med Imaging 2020;39:3029–3041. [PubMed: 32275585]
64. Gottwald LM, Blanken CPS, Tourais J, et al. Retrospective camera-based respiratory gating in clinical whole-heart 4D flow MRI. J Magn Reson Imaging 2021;54:440–451. [PubMed: 33694310]
65. Chikop SA, Anchan ABS, Koulagi G, Honnedevasthana AA, Imam S, Geethanath S. Automatic motion correction of musculoskeletal MRI using DSLR camera. Magn Reson Imaging 2018;48(April 2017):74–79. [PubMed: 29307810]
66. Harder F, Lohöfer FK, Kaissis GA, et al. Camera-based respiratory triggering improves the image quality of 3D magnetic resonance cholangiopancreatography. Eur J Radiol 2019;120(September): 108675. [PubMed: 31585303]

67. Chen B, Weber N, Odille F, et al. Design and validation of a novel MR-compatible sensor for respiratory motion modeling and correction. IEEE Trans Biomed Eng 2017;64:123–133. [PubMed: 27046890]
68. Preiswerk F, Toews M, Cheng C, et al. Hybrid MRI-ultrasound acquisitions, and scannerless real-time imaging. Magn Reson Med 2017;78: 897–908. [PubMed: 27739101]
69. Madore B, Cheng C, Preiswerk F. Combining MR and ultrasound imaging, through sensor-based probe tracking. In Proceedings of the 27th International Society of Magnetic Resonance in Medicine, Montreal, Canada; 2019, 0968.
70. Madore B, Preiswerk F, Bredfeldt J, Zong S, Cheng C. Motion monitoring using MR-compatible ultrasound-based sensors. In Proceedings of the 28th International Society of Magnetic Resonance in Medicine, virtual; 2020, 0461.
71. Cuthbertson J, Truong TK, Yadav V, Robb F, Song A, Darnell D. Dual-stream iPRES-W head coil array for MR imaging, wireless respiratory tracking, and wireless localized B0 shimming. In Proceedings of the 28th International Society of Magnetic Resonance in Medicine. virtual; 2020, 1262.
72. Willey D, Bresticker J, Truong TK, Song A, Madore B, Darnell D. Integrated RF/wireless coil and ultrasound-based sensors to enable wireless physiological motion monitoring in MRI. In Proceedings of the 28th International Society of Magnetic Resonance in Medicine, virtual; 2020, 1282.
73. Stockmann JP, Wald LL. In vivo B_0 field shimming methods for MRI at 7T. Neuroimage 2018;168:71–87. [PubMed: 28602943]
74. de Graaf RA, Juchem C. B_0 shimming technology. In: Webb AG, editor. Magnetic resonance technology: Hardware system component design: Cambridge, UK: Royal Society of Chemistry; 2016. p 166–207.
75. Juchem C, Brown PB, Nixon TW, et al. Dynamic multi-coil shimming of the human brain at 7 T. J Magn Reson 2011;212:280–288. [PubMed: 21824794]
76. Aghaeifar A, Mirkes C, Bause J, et al. Dynamic B_0 shimming of the human brain at 9.4 T with a 16-channel multi-coil shim setup. Magn Reson Med 2018;80(4):1714–1725. [PubMed: 29424461]
77. Han H, Song AW, Truong TK. Integrated parallel reception, excitation, and shimming (iPRES). Magn Reson Med 2013;70(1):241–247. [PubMed: 23629974]
78. Truong TK, Darnell D, Song AW. Integrated RF/shim coil array for parallel reception and localized B_0 shimming in the human brain. Neuroimage 2014;103:235–240. [PubMed: 25270602]
79. Stockmann JP, Witzel T, Keil B, et al. A 32-channel combined RF and B_0 shim array for 3T brain imaging. Magn Reson Med 2016;75(1): 441–451. [PubMed: 25689977]
80. Twieg M, Mehta BB & Handa S et al. The MRF array: An iPRES coil array for accelerated magnetic resonance fingerprinting. In: Proceedings of the 26th Annual Meeting of ISMRM, 2018;26:137.
81. Boer VO, Pedersen JO & Andreasen H et al. Shielded coaxial cable coils for transmit, receive and B0 shimming in a 7T neck array. In: Proceedings of the 29th annual meeting of ISMRM, 2021;29:3109.
82. Darnell D, Truong TK, Song AW. Integrated parallel reception, excitation, and shimming (iPRES) with multiple shim loops per RF coil element for improved B_0 shimming. Magn Reson Med 2017;77(5):2077–2086. [PubMed: 27174387]
83. Ma Y, Darnell D, Zhang H, Song AW & Truong TK. Integrated parallel reception, excitation, and shimming (iPRES) breast coil array for simultaneous MR image acquisition and localized B0 shimming. In: Proceedings of the 26th Annual Meeting of ISMRM, 2018;26:842.
84. Cuthbertson JD, Darnell D, Stormont R, Robb F, Song AW & Truong TK. A 4-channel iPRES-W AIR coil array for simultaneous MR image acquisition and wirelessly-controlled localized B0 shimming of the spinal cord. In: Proceedings of the 27th Annual Meeting of ISMRM, 2019;27:1489.
85. Esmaeili M, Stockmann J, Strasser B, et al. An integrated RF-receive/B_0-shim array coil boosts performance of whole-brain MR spectroscopic imaging at 7 T. Sci Rep 2020;10:15029. [PubMed: 32929121]

86. Willey D, Darnell D, Song AW, Truong TK. Application of an integrated radio-frequency/shim coil technology for signal loss recovery in fMRI. Magn Reson Med 2021, in press. 10.1002/mrm.28925.
87. Liao C, Stockmann J, Tian Q, et al. High fidelity, high-isotropic-resolution diffusion imaging through gSlider acquisition with B_1^+ and T_1 corrections and integrated ΔB_0/Rx shim array. Magn Reson Med 2020;83:56–67. [PubMed: 31373048]
88. Liao C, Bilgic B, Tian Q, et al. Distortion-free, high-isotropic-resolution diffusion MRI with gSlider BUDA-EPI and multicoil dynamic B_0 shimming. Magn Reson Med 2021;86:791–803. [PubMed: 33748985]
89. Darnell D, Ma Y, Wang H, Robb F, Song AW, Truong TK. Adaptive integrated parallel reception, excitation, and shimming (iPRES-A) with microelectromechanical system switches. Magn Reson Med 2018;80 (1):371–379. [PubMed: 29148102]
90. Ma Y, Bresticker J, Darnell D, Robb F, Song AW & Truong TK. Adaptive iPRES body coil array with microelectromechanical system switches for simultaneous imaging and localized B0 shimming. In: Proceedings of the 28th Annual Meeting of ISMRM, 2020;28:4226.
91. Arango N, Stockmann J, Adalsteinsson E & White J. Computational shim coil design applied to augmenting a shim array with a non-eye-occluding face plate. In: Proceedings of the 28th Annual Meeting of ISMRM, 2020;28:4224.
92. Zhou J, Stockmann JP, Arango N, et al. The orthogonal shim coil for 3T brain imaging. Magn Reson Med 2019;83(4):1499–1511. [PubMed: 31631391]
93. Manhard MK, Stockmann J, Liao C, et al. A multi-inversion multi-echo spin and gradient echo echo planar imaging sequence with low image distortion for rapid quantitative parameter mapping and synthetic image contrasts. Magn Reson Med 2021;86:866–880. [PubMed: 33764563]
94. Topfer R, Foias A & Rios L et al. Integrated B0/Rx coil array for improved spinal cord imaging at 3T. In: Proceedings of the 26th Annual Meeting of ISMRM, Paris; 2018;26:834.
95. Topfer R, Rios NL & Foias A et al. Real time shimming in the cervical spinal cord using an 8-channel AC/DC array and a capacitive respiratory sensor. In: Proceedings of the 27th Annual Meeting of ISMRM, Montreal; 2019;27:925.
96. Gao Y, Mareyam A, Sun Y, et al. A 16-channel AC/DC array coil for anesthetized monkey whole-brain imaging at 7T. Neuroimage 2020; 207:116396. [PubMed: 31778818]
97. Thompson Z, Darnell D, Morozov D, Beeman SC, Song AW & Truong TK. Numerical optimization of an iPRES coil design for high SNR and localized B0 shimming performance in small animal imaging. In: Proceedings of the 28th Annual Meeting of ISMRM, 2020;28:4230.
98. Stockmann J, Arango NS & Poser B et al. Spatially-selective excitation using a tailored nonlinear ΔB0 pattern generated by an integrated multi-coil ΔB0/Rx array. In: Proceedings of the 26th Annual Meeting of ISMRM, Paris; 2018;26:170.
99. Xu J, Arango N & Liao C et al. Lipid artifact removal by dynamic shimming (LARDS) with multi-coil B0 shim arrays. In: Proceedings of the 29th meeting of ISMRM, 2021;29:782.
100. Craven-Brightman L, Chang Y & Witzel T et al. Regulating labeling e! ciency in arterial spin labeling using a multi-coil B0 shim array: Application to territory mapping. In: Proceedings of the 29th annual meeting of ISMRM, 2021: 29:469.
101. Guerin B, Milshteyn E & Chang Y et al. “Universal” non-selective pulse design at 7 Tesla using a birdcage coil and a B0 shim array: Evaluation of kT-points and fully optimized pulses. In: Proceedings of the 29th annual meeting of ISMRM, 2021;29:3949.
102. Mehta BB, Twieg M & Yang M et al. Improving uniqueness of magnetic resonance fingerprinting (MRF) signal evolutions using spatiotemporal variation of non-linear ΔB0 shim coil. In: Proceedings of the 26th Annual Meeting of ISMRM, 2018;26:1019.
103. Xu J, Stockmann J & Bilgic B et al. Multi-frequency wave-encoding (mf-wave) on gradients and multi-coil shim-array hardware for highly accelerated acquisition. In: Proceedings of the 28th Annual Meeting of ISMRM, 2020;28:618.
104. Huellner MW. PET/MR in head and neck cancer—An update. Semin Nucl Med 2021;51:26–38. [PubMed: 33246536]

105. Guberina N, Hetkamp P, Ruebben H, et al. Whole-body integrated [68Ga]PSMA-11-PET/MR imaging in patients with recurrent prostate cancer: Comparison with whole-body PET/CT as the standard of reference. Mol Imaging Biol 2020;22:788–796. [PubMed: 31482413]

106. Klain M, Nappi C, Nicolai E, et al. Comparison of simultaneous 18F-2-[18F] FDG PET/MR and PET/CT in the follow-up of patients with differentiated thyroid cancer. Eur J Nucl Med Mol Imaging 2020;47: 3066–3073. [PubMed: 32601803]

107. Larsson K, Halvarsson B, Singh D, et al. High-speed beam tracking demonstrated using a 28 GHz 5G trial system. In: 2017 IEEE 86th Vehicular Technology Conference; 2017, 1–5.

108. Alluhaibi O, Kampert E, Jennings PA, Higgins MD. Impact of overlapped AoAs on the achievable uplink rate of hybrid beamforming for massive MIMO mm-wave systems for industrial environments. IEEE Access 2019;7:101178–101194.

109. Sung M, Lee JH, Kim J, et al. RoF-based radio access network for 5G mobile communication systems in 28 GHz millimeter-wave. J Light Technol 2020;38:409–420.

110. Rösch J, Mennecke A, Knott M, Doerfler A, Grodzki DM. Quiet FLAIR at 7T MRI. Invest Radiol 2020;55:722–726. [PubMed: 32516159]

111. Juchem C, Theilenberg S, Kumaragamage C, et al. Dynamic multicoil technique (DYNAMITE) MRI on human brain. Magn Reson Med 2020; 84:2953–2963. [PubMed: 32544274]

112. Scheffler K, Loktyushin A, Bause J, Aghaeifar A, Steffen T, Schölkopf B. Spread-spectrum magnetic resonance imaging. Magn Reson Med 2019;82:877–885. [PubMed: 31025413]

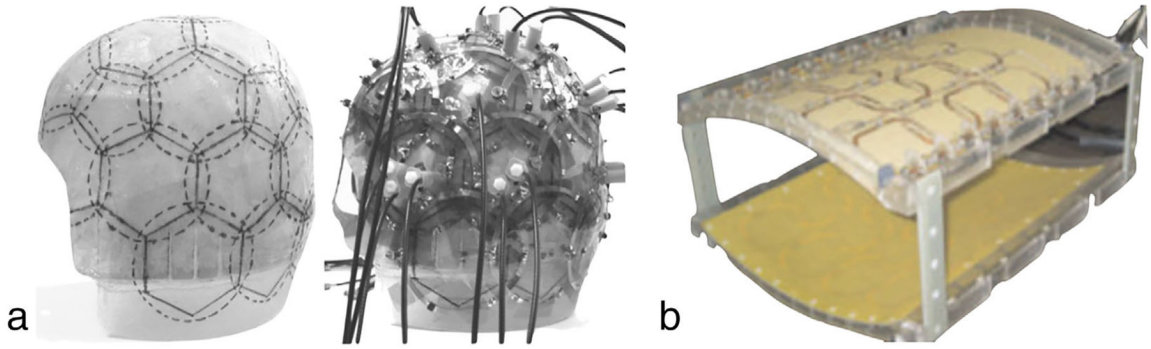

FIGURE 1:
Thirty-two-channel “soccer ball” (a) and body (b) coil arrays placed on rigid enclosures for neuro and body imaging. Adapted from Refs. 8 and 19, respectively, with permission.

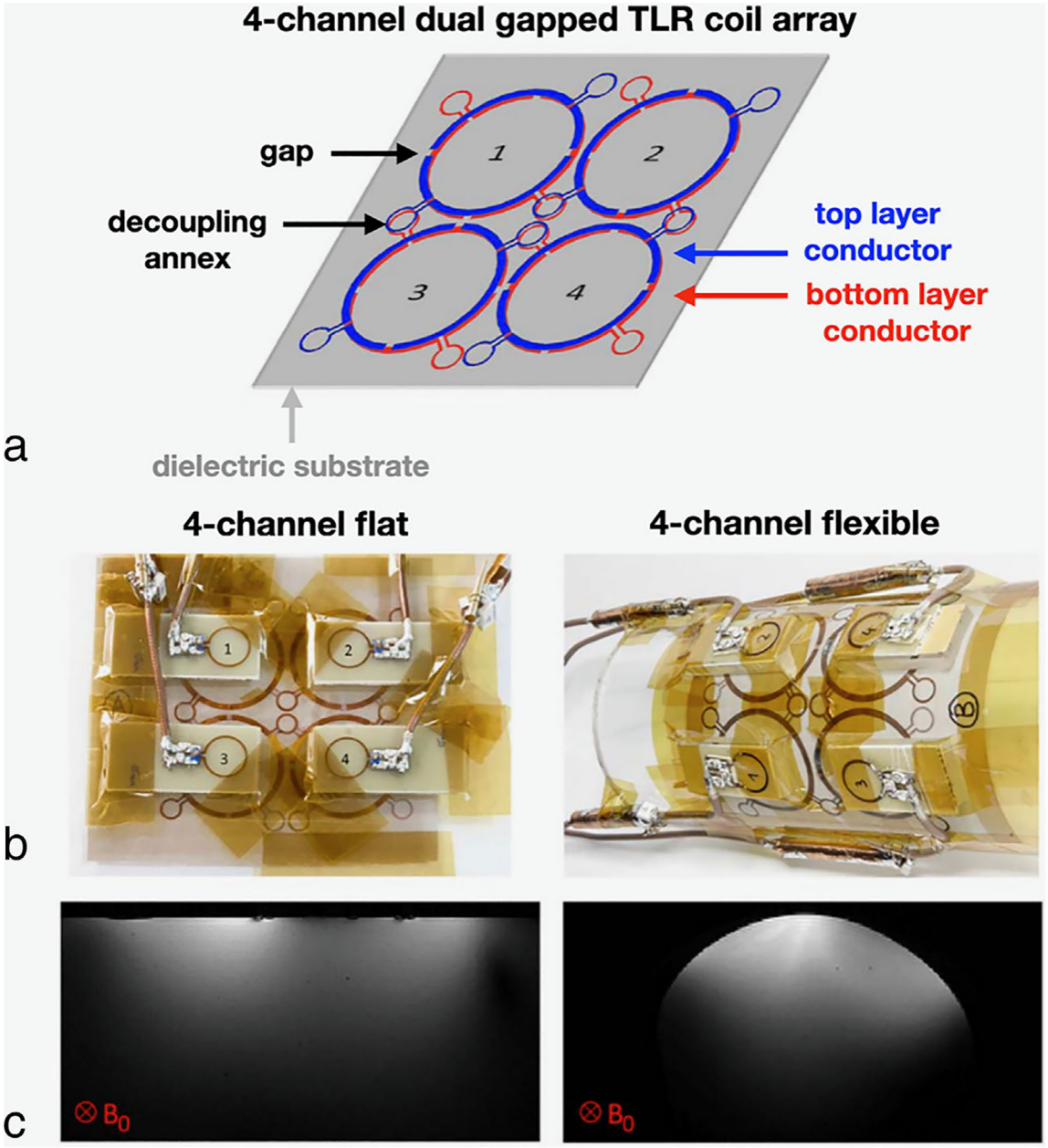

FIGURE 2:
Four-channel dual gapped TLR coil design with decoupling annexes (a) in a flat or flexible configuration (b) to image a flat or curved phantom (c), respectively. Adapted from Ref. 13, with permission.

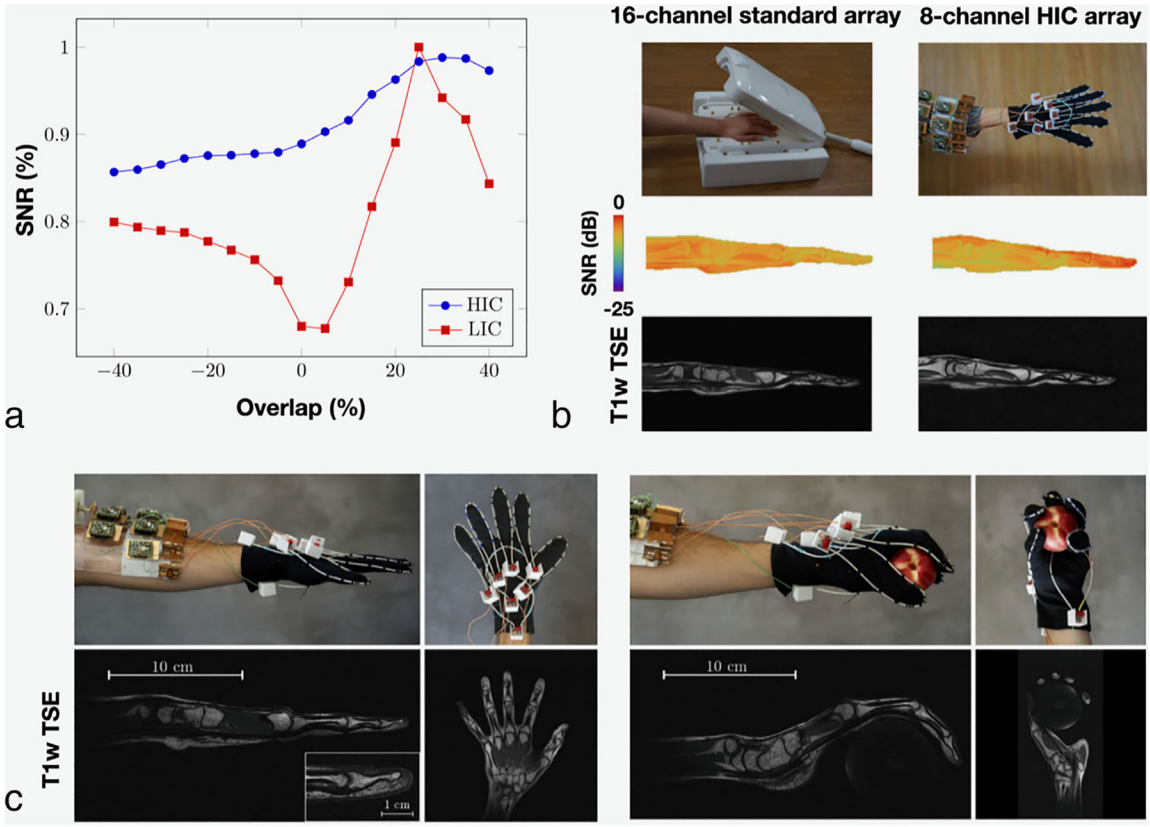

FIGURE 3:

(a) Critical overlap of HIC and standard coil elements. T_1-weighted TSE images of a wrist acquired with an eight-channel HIC coil array to compare the SNR with that of a 16-channel standard coil array (b) and holding a peach to demonstrate its flexibility (c). Adapted from Ref. 11, with permission.

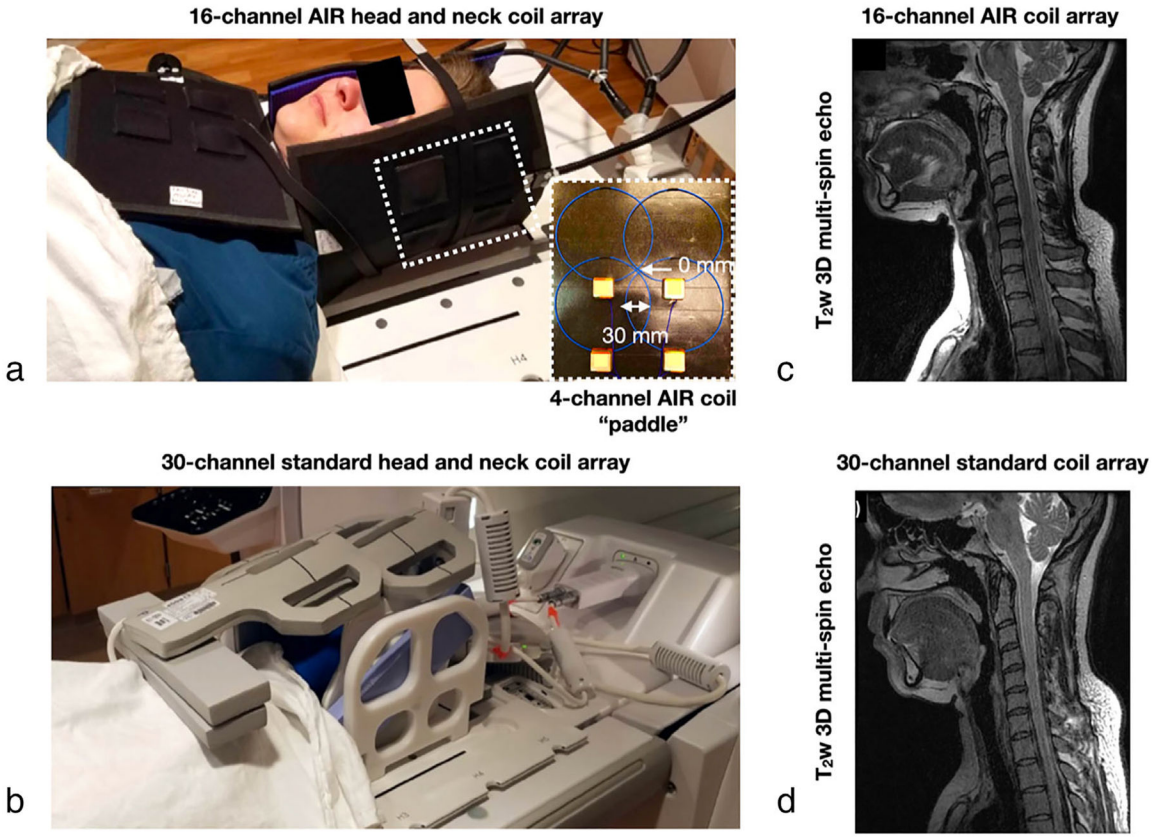

FIGURE 4:

T_2-weighted 3D multi-spin echo images acquired with a 16-channel AIR head and neck coil array (a) and a 30-channel standard head and neck coil array (b). The AIR coil array (c) provided a similar diagnostic image quality as the standard coil array (d). The overlap between the AIR coil elements ranged from 0 to 30 mm. Adapted from Ref. 30, with permission.

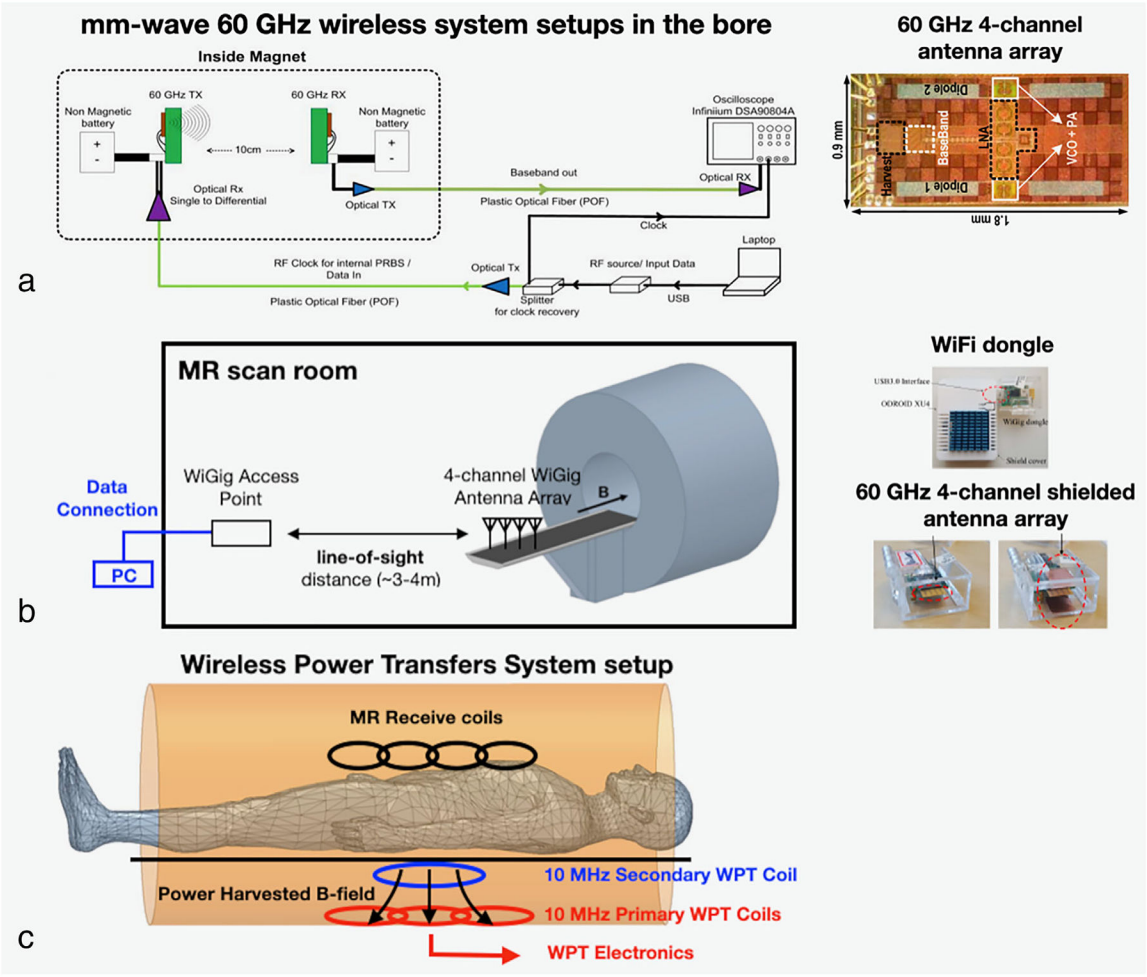

FIGURE 5:

Sixty-GHz wireless data transfer systems using either custom (a) or off-the-shelf (b) electric components and antennas. With data rates above 500 Mbps, they are suitable for wireless MRI data transfer for high-density coil arrays. The array electronics can potentially be powered using wireless power transfer from the system (c). (a–b) adapted from Refs. 38 and 47, respectively, with permission.

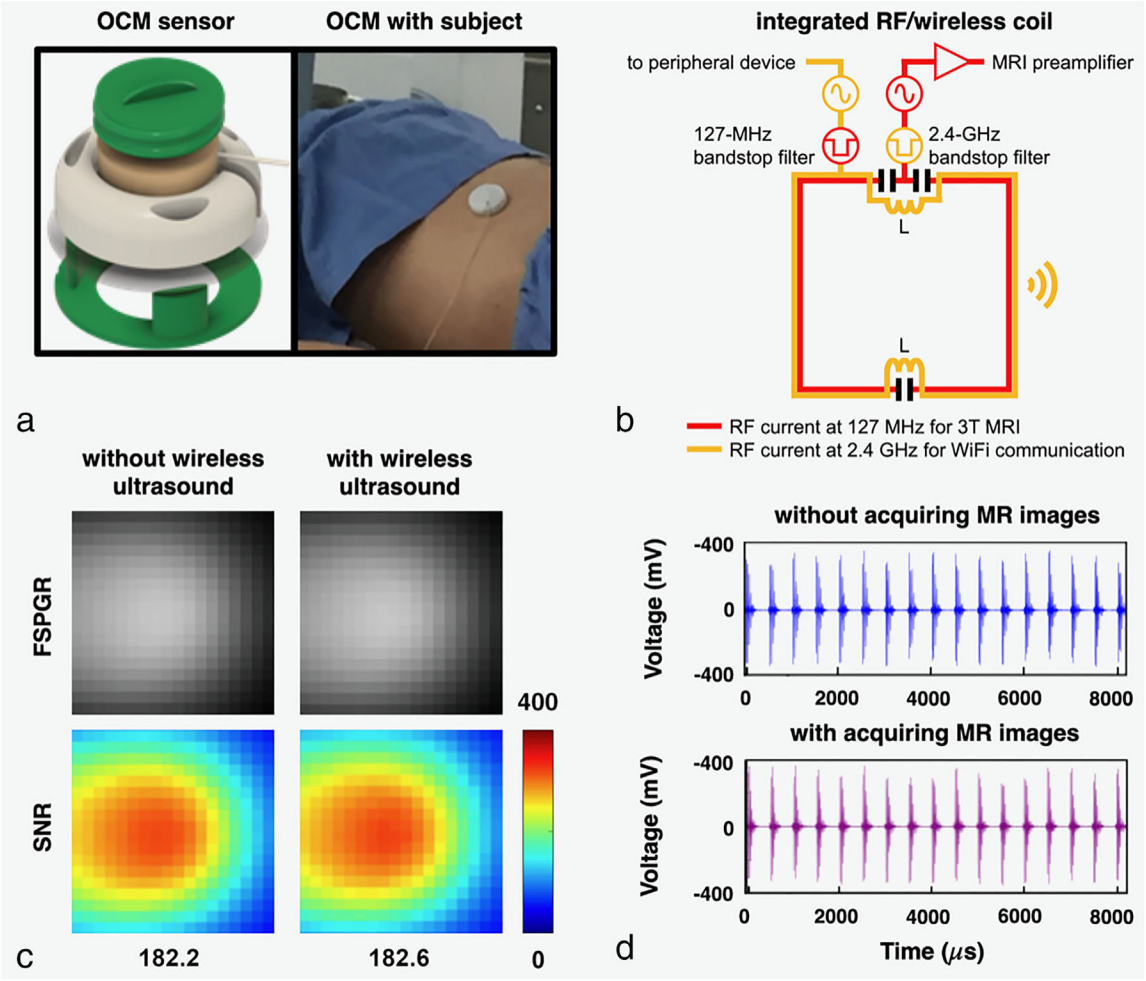

FIGURE 6:

Novel OCM ultrasound probe (a) used with an integrated RF/wireless coil (b) in the scanner bore to simultaneously acquire MRI images and wirelessly transmit ultrasound data on a phantom with no loss in SNR (c) or ultrasound data quality (d).

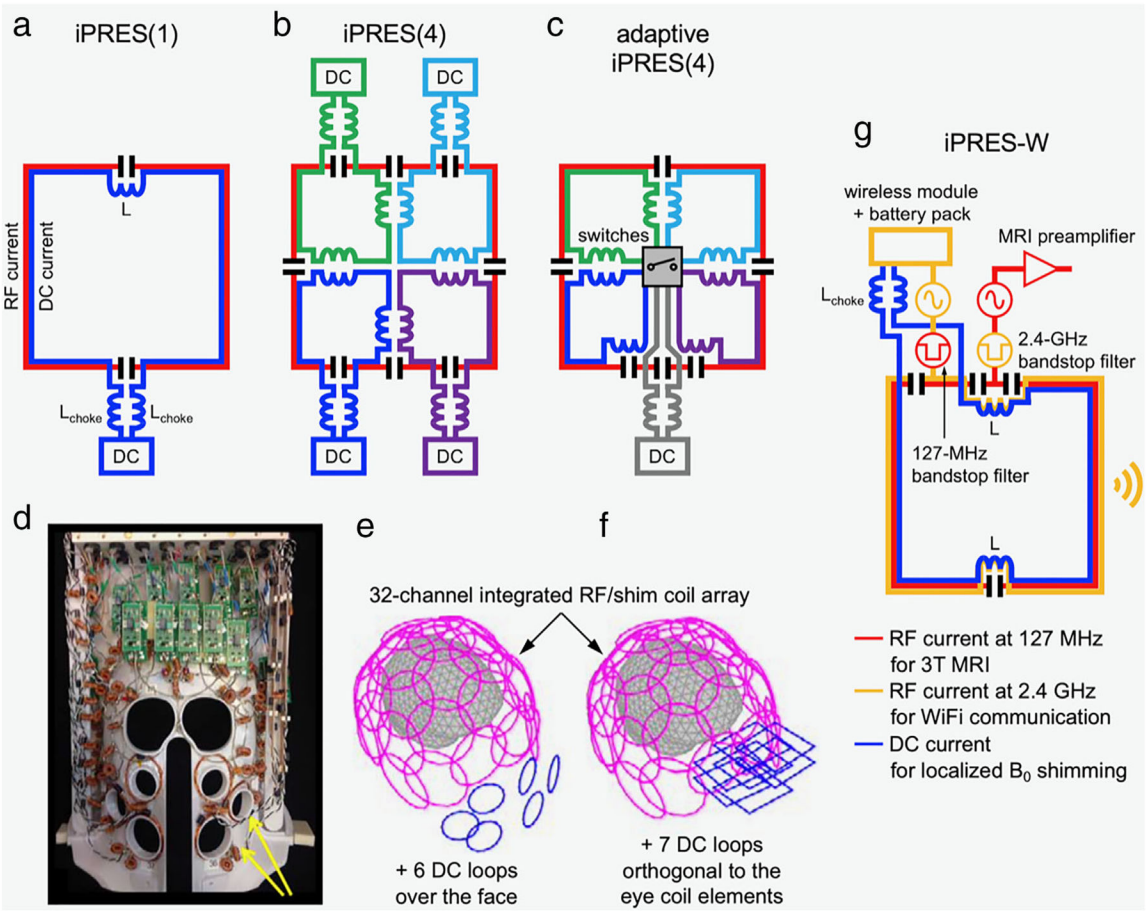

FIGURE 7:

Examples of integrated RF/shim coil designs. (a) iPRES(1) coil element with a DC power supply, a pair of chokes (L_{choke}), and an inductor (L) to enable a DC current (blue) to flow on the coil element for localized B_0 shimming in addition to the RF current (red) for RF excitation/reception. (b) iPRES(4) coil element split into four smaller RF-isolated DC loops, each with an independent DC current. (c) Adaptive iPRES(4) coil element with switches to direct the DC current from a single DC power supply to the appropriate DC loops for shimming. Thirty-two-channel integrated RF/shim head coil array with additional four-turn DC loops over the face (d,e) or orthogonal to the eye coil elements (f). (g) iPRES-W coil element with high-impedance 127-MHz and 2.4-GHz bandstop filters between the coil element and the wireless module or the MRI preamplifier, respectively, to enable an RF current within the 2.4-GHz WiFi communication band (orange) to flow on the coil element for wireless communication in addition to the RF current at the 127-MHz Larmor frequency (red) for 3T MRI and the DC current (blue) supplied by an on-board MR-compatible battery pack for localized B_0 shimming. (d) and (e,f) adapted from Refs. 73 and 92, respectively, with permission.

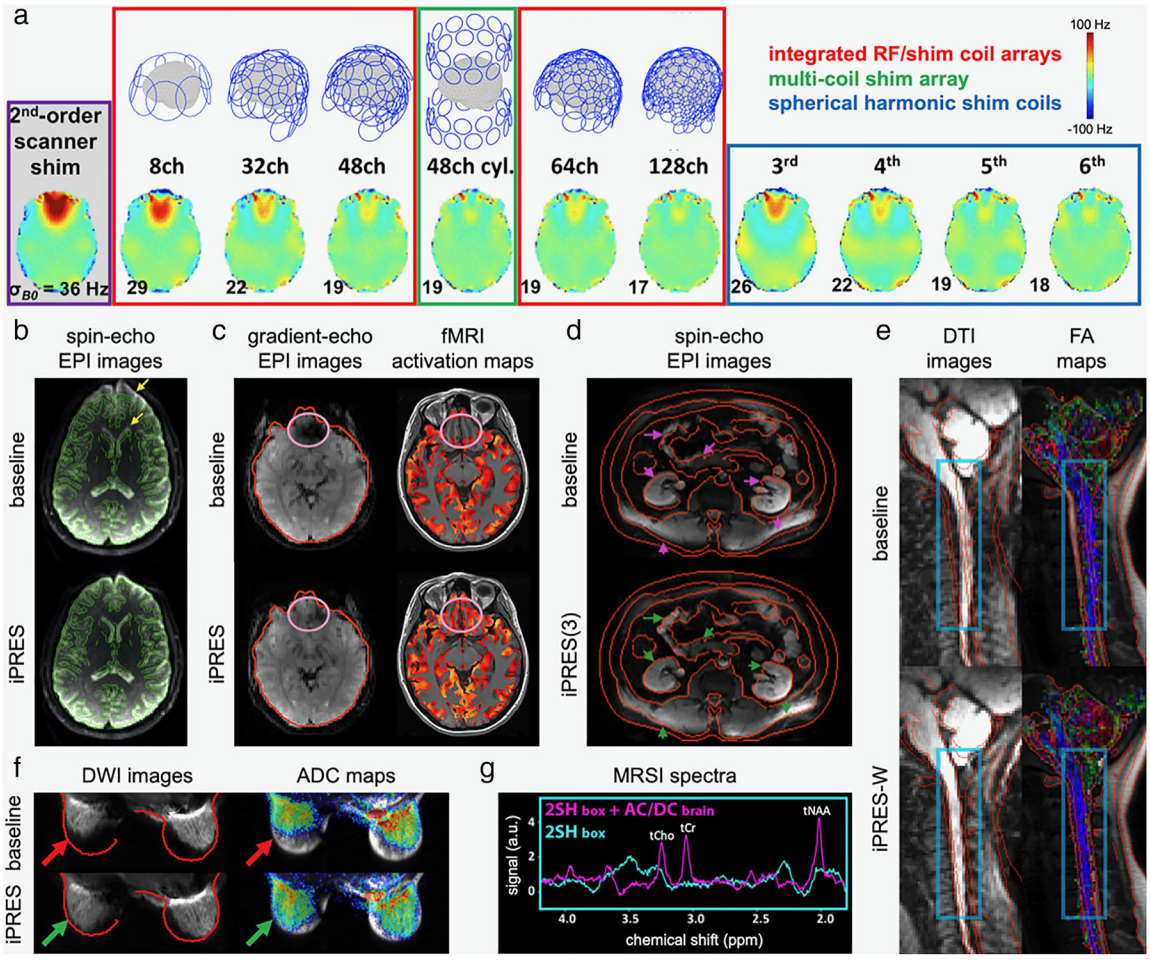

FIGURE 8:

Localized B_0 shimming applications of integrated RF/shim coil arrays. (a) ΔB_0 maps of the human brain at after slice-optimized shimming with different integrated RF/shim coil arrays (red), a multi-coil shim array (green), and third- to sixth-order SH shim coils (blue). (b) Spin-echo EPI images of the brain overlaid with contour lines from an undistorted anatomical image, showing substantially reduced distortions after slice-optimized shimming with iPRES compared to whole-brain second-order SH shimming. (c) Gradient-echo EPI images and breath-holding fMRI activation maps, showing a higher signal intensity and number of activated voxels in the inferior frontal brain region (pink oval) after slice-optimized shimming with iPRES. (d) Spin-echo EPI images of the abdomen, (e) DTI images and fractional anisotropy (FA) maps of the spinal cord, and (f) DWI images and apparent diffusion coefficient (ADC) maps of the breast, all showing reduced distortions after slice-optimized shimming with an iPRES(3) body coil array, an iPRES-W spine coil array, and an iPRES breast coil array, respectively. (g) MRSI spectra in a frontal brain region, showing improved metabolic peaks after shimming with an integrated RF/shim coil array. (a–g) adapted from Refs. 79, 78, 86, 82, 84, 83 and 85, respectively, with permission.

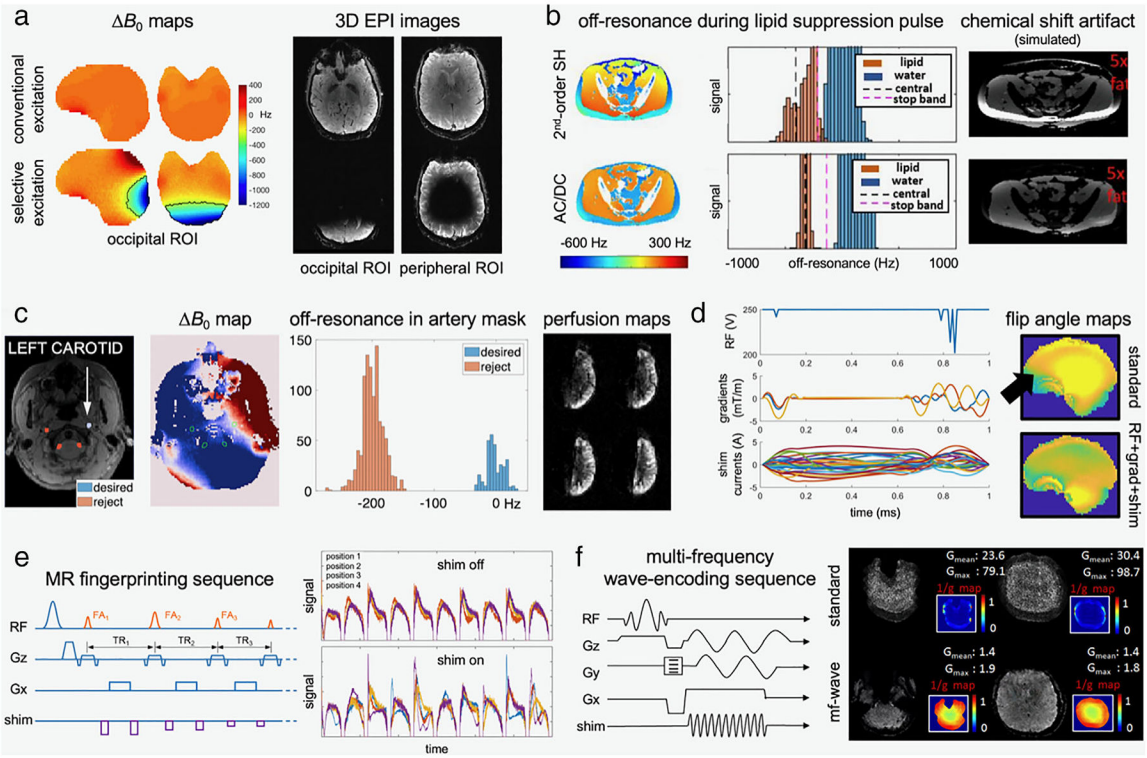

FIGURE 9:

Nonshimming applications of integrated RF/shim coil arrays. (a) Spatially selective excitation using a tailored nonlinear ΔB_0 pattern during the RF excitation to enable zoomed 3D EPI in the visual cortex or peripheral cerebrum. (b) Improved lipid suppression in MRSI using a tailored ΔB_0 offset during the lipid suppression RF pulse to better separate the lipid and water peaks and reduce chemical shift artifacts. (c) Cerebral blood flow territory mapping with ASL using a tailored ΔB_0 field near specific arteries during the labeling RF pulses to selectively label the spins in the desired artery (eg, left carotid). (d) Flip-angle uniformization at 7T using a joint optimization of the RF waveform, $x/y/z$ gradient waveforms, and shim waveforms from an integrated RF/shim coil array. (e) Improved encoding capabilities and uniqueness of signal evolutions in MR fingerprinting using additional spatiotemporal ΔB_0 variations throughout the pulse sequence. (f) Accelerated multi-frequency wave-encoding (mf-wave) using additional high-frequency wave-encoding of the shim waveforms from an integrated RF/shim coil array during the data acquisition. (a–f) adapted from Refs. 98–103, respectively, with permission.